RSC Chemical Biology

ROYAL SOCIETY OF CHEMISTRY

PAPER

View Article Online
View Journal | View Issue

Cite this: *RSC Chem. Biol.*, 2025, **6**, 1465

Unravelling structure–function interactions between fluorinated heparan sulfate mimetics and signaling proteins†

Virendrasinh Mahida,‡[a] Rakesh Raigawali,‡[a] Paula González,[b] Ana Gimeno,[bc] Shani Leviatan Ben-Arye,[e] Saurabh Anand,[a] Sandhya Mardhekar,[a] Jesús Jiménez-Barbero,*[bcd] Vered Padler-Karavani*[e] and Raghavendra Kikkeri*[a]

Received 5th July 2025,
Accepted 10th July 2025

DOI: 10.1039/d5cb00174a

rsc.li/rsc-chembio

Fluorinated carbohydrates are emerging scaffolds in glycobiology, enabling the elucidation of the roles of the individual hydroxyl groups of a carbohydrate in protein binding and drug discovery. Herein, we report a divergent strategy to synthesize seven heparan sulfate (HS) mimetics featuring a fluorine atom at the C3 position of the glucuronic acid residue, with the objective of modulating structure–function relationships. The sensitivity of fluorine signals to sulfation patterns was confirmed *via* ^{19}F-NMR spectroscopy, while $^{3}J_{HH}$ coupling and NOE data demonstrated that the glucuronic acid residue retained its $^{4}C_{1}$ conformation. Glycan microarray analysis and SPR binding studies revealed that a single hydroxyl-to-fluorine substitution in HS mimetics retains the binding of *N*-acetylated HS sequences for several growth factors and chemokines. Remarkably, GlcNAc6S-GlcA(3F) and GlcNS6S3S-GlcA(3F) exhibited binding properties comparable to those of highly *N*-sulfated native HS ligands. These findings provide valuable insights for the development of novel therapeutic agents targeting morphogens and cell signalling pathways.

Heparan sulfate (HS) is an anionic polysaccharide that interacts with a wide variety of proteins, orchestrating cell signalling and disease progression.[1] Routinely, HS binds to growth factors and regulates cell signalling pathways that drive processes like cell proliferation, differentiation, and angiogenesis.[2] It also binds to chemokines, facilitating immune surveillance and tissue repair.[3] Viruses, such as SARS-CoV-2, HSV-1, and dengue virus, exploit HS as a receptor for infection or a co-receptor to evade the immune system.[4] These striking properties make HS ligands attractive targets for therapeutic and diagnostic applications.

HS structures comprise repeating disaccharide units of glucosamine and uronic acids, most notably the conformationally flexible L-iduronic acid. The HS chains display considerable diversity in both sulfation patterns and chain lengths,[1–3] creating millions of distinct structural variants.[5] However, structure–function relationship studies with synthetic HS glycans revealed that a single HS structure is often bound by several different proteins, limiting its usage in diagnostics or therapy. For example, 3-*O*-sulfated HS oligosaccharides with uronic acids participate in anticoagulation activity, neurite growth factor binding, and HSV-1 virus attachment.[6] Likewise, *N*-sulfated L-iduronic acid-based HS glycans are critical for binding to VEGF, but also for binding to chemokines such as CCL2 and CCL5, and the SARS-CoV-2 spike protein.[7] To address these limitations, HS mimetics are synthesized, where isostructural sugars are substituted on the HS backbone to alter the biological activities. For example, L-iduronic acid in the idraparinux drug was substituted with D-glucuronic acid, D-xylose, 6-deoxy-L-talose, and even $^{1}C_{4}$ and $^{2}S_{0}$-conformation locked L-iduronic acid moieties to study the anticoagulant activity of this drug.[8] Alternatively, molecular editing of hydroxyl groups with fluorine atoms has been extensively employed in carbohydrate chemistry to develop glycomimetics. Replacing C–OH bonds with C–F bonds in glycans induces several beneficial effects, including enhanced lipophilicity, improved cellular permeability, and increased stability against hydrolytic cleavage of glycosidic bonds.[9] The bioisosteric replacement of hydroxyl groups by

[a] *Department of Chemistry, Indian Institute of Science Education and Research, Pune, 411008, India. E-mail: rkikkeri@iiserpune.ac.in*
[b] *CIC bioGUNE, Basque Research Technology Alliance, BRTA, Bizkaia Technology park, 48160 Derio, Spain. E-mail: jjbarbero@cicbiogune.es*
[c] *Ikerbasque, Basque Foundation for Science, 48009 Bilbao, Spain*
[d] *Dept. Organic Chemistry II, Faculty of Science and Technology, UPV-EHU, 48940, Leioa, Spain*
[e] *Department of Cell Research and Immunology, The Shmunis School of Biomedicine and Cancer Research, The George S. Wise Faculty of Life Sciences, Tel Aviv University, Tel Aviv, 69978, Israel. E-mail: vkaravani@tauex.tau.ac.il*

† Electronic supplementary information (ESI) available. See DOI: https://doi.org/10.1039/d5cb00174a

‡ These authors contributed equally to this work.

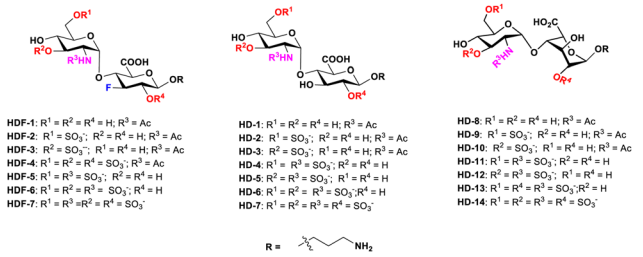

Fig. 1 Chemical structures of 7-fluorinated D-glucuronic acid based HS mimetics (**HDF-1** to **HDF-7**) and 14 native HS disaccharides (D-glucuronic acid based **HD-1** to **HD-7** and L-iduronic acid based **HD-8** to **HD14)**.

fluorine atoms preserves the hydrogen acceptor nature of carbohydrates, while the ionic nature of the C–F(δ^-) bond stabilizes electrostatic interactions with adjacent electropositive groups, potentially modulating carbohydrate–protein interactions.[9h] Furthermore, the incorporation of fluorine enables ^{19}F-NMR monitoring, facilitating direct detection of metabolic stability and carbohydrate–protein interactions.[10] Recent studies on GM_1, galectin-specific ligands, and Lewis X glycan that were systematically modified with fluorine atoms have demonstrated the potential of fluorination to fine-tune carbohydrate–protein interactions.[9e–g,10] Therefore, fluorinated HS mimetics are postulated to fine-tune the microenvironment of carbohydrate–protein interactions, thereby enabling the development of small, selective ligands targeting HS-binding proteins. Herein, we present the design, synthesis and conformational analysis of seven fluorinated HS disaccharide mimetics and native HS disaccharides (Fig. 1), followed by high-throughput glycan microarray binding studies of several growth factors and chemokines. Disaccharide analogs were selected for this initial proof-of-concept study to optimize the synthetic methodology and investigate how minimal structural units can reflect binding variations with growth factors and chemokines, driven by differences in sulfation patterns and the uronic acid configuration.[14,15a] Our results demonstrate that the incorporation of fluorine atoms within the *N*-acetate domains of HS mimetics preserves their binding preferences and, in some cases, also leads to increased binding when compared to their *N*-sulfated counterparts. Comprehensive conformational analyses, molecular docking simulations, surface plasmon resonance (SPR) assays, fibroblast growth factor 2 (FGF2)-induced cell proliferation studies, and mitogen-activated protein kinase (MAPK) signalling assays collectively support these observations. Together, our findings underscore the potential of fluorinated HS analogues as next-generation tools for therapeutic and diagnostic applications, offering a novel avenue for targeting HS-mediated biological processes with improved precision.

Results and discussion

Fluorinated HS disaccharides with regioselective *N*-acetylated or *N*-sulfated and *O*-sulfated analogues were synthesized from disaccharide building blocks **16a** and **16b** using a divergent synthetic approach described in Scheme 1. The synthesis of disaccharides **16a**/**16b** required 3-fluoro-3-deoxy glucose **12** and glucosamine building blocks **13a**/**13b**[11] with orthogonal protecting groups to control regioselective glycosylation and sulfation patterns. The 3-fluoro-3-deoxy-D-glucose building block **12** was derived from 1,2 : 5,6-*O*-isopropylidene-α-D-allofuranose as the starting material, employing a standard procedure (Scheme 1).[9d] Glycosylation of donor **13a**/**13b** with acceptor **12** in the presence of NIS and TMSOTf yielded the α-disaccharides **14a** and **14b**, respectively. Mild thiourea and pyridine-catalyzed deprotection of chloroacetate groups, followed by oxidation using the catalytic 2,2,6,6-tetramethylpiperidinyloxyl (TEMPO) free radical in the presence of excess [bis(acetoxy)iodo]benzene (BAIB), was carried out. This was followed by methyl iodide and potassium bicarbonate-mediated esterification, resulting in disaccharides **16a** and **16b**, respectively (Scheme 1).

Next, TBDPS or NAP groups were selectively removed using 70% HF.Py or DDQ, followed by sulfation with the SO_3-TEA complex to afford 6-*O*-sulfated and 3-*O*-sulfated derivatives **18** and **19**, respectively. Subsequently, lithium hydroxide mediated ester hydrolysis and $Pd(OH)_2$ catalyzed hydrogenolysis yielded **HDF2** and **HDF3**. Cleavage of TBDPS, Bz, and 2-NAP groups of **16a**/**16b**, followed by either non-sulfation or sulfation using the SO_3–TEA complex, and subsequent global deprotection yielded **HDF1** and **HDF4**, respectively (Scheme 1). For the *N*-sulfated series, **16b** underwent chemoselective cleavage of TBDPS, Bz, and 2-NAP groups, followed by *O*-sulfation, and subsequently, the azide group was converted to amines using trimethylphosphine. *N*-Sulfation was achieved using the SO_3.Py complex, followed by global deprotection (Scheme 2). The non-fluorinated HS disaccharides comprising of D-glucuronic acid (**HD-1** to **HD-7**) and L-iduronic acid based (**HD-8** to **HD-14**) were synthesized and characterized using a divergent strategy, as previously described.[11d]

The conformation of the fluorinated HS disaccharides with different sulfation patterns was analyzed using NMR spectroscopy. Due to the high structural similarity of the six fluorinated compounds synthesized, representative NMR analysis of **HDF-7** is detailed in Fig. 2(i) and (ii). The NMR spectrums of

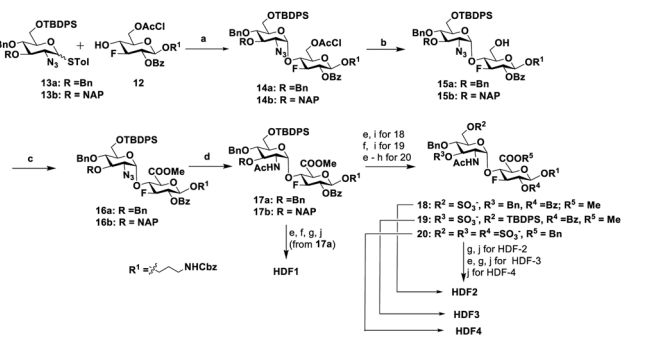

Scheme 1 Synthesis of glucuronic acid based HS disaccharides: (a) NIS, TMSOTf, DCM, −78 °C, 15 min; (b) thiourea, Py : MeOH (1 : 1), 80 °C, 2 h; (c) (i) TEMPO, BAIB, DCM : H_2O(1 : 1), RT; (ii) MeI, K_2CO_3, DMF, 6 h, RT; (d) Zn dust, THF : AcOH : Ac_2O (3 : 2 : 1), RT, 12 h; (e) HF.Py, Py, 0 °C, 12 h; (f) DDQ, DCM : H_2O (18 : 1), RT, 1 h; (g) LiOH, H_2O : THF(1 : 1), RT, 12 h; (h) BnBr, $NaHCO_3$, DMF, 60 °C, 2 h; (i) SO_3.Et_3N, DMF, 60 °C, 48–72 h; and (j) H_2, $Pd(OH)_2$, H_2O, RT, 48 h.

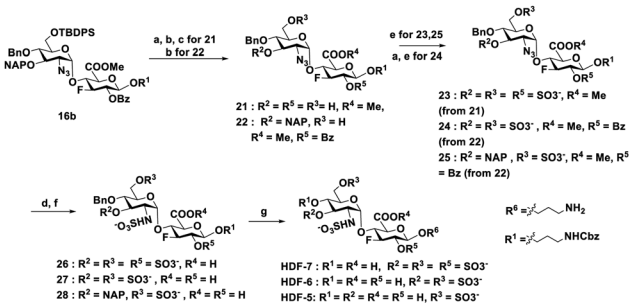

Scheme 2 Synthesis of fluorinated *N*-sulfated HS disaccharides: (a) DDQ, DCM : H_2O (18 : 1), RT, 1 h; (b) HF.Py, Py, 0 °C, 12 h; (c) NaOMe, MeOH, RT, 6 h; (d) LiOH, H_2O : THF(1 : 1), RT, 12 h; (e) SO_3.Et_3N, DMF, 60 °C, 48–60 h; (f) (i) PMe_3.THF, RT, 24 h; (ii) SO_3.Py. MeOH, 1 M NaOH, 0 °C, 48 h; and (g) H_2, $Pd(OH)_2$, H_2O, RT, 48 h.

HDF1-3 and **HDF5-6** and information of all analyzed compounds are included in Sections S4–S6, ESI.†

All compounds displayed well-dispersed NMR signals, facilitating resonance assignment. While the presence of fluorine was ascertained by 1D ^{19}F NMR spectroscopy, the information gathered from HSQC and ^{19}F-relay-[H]H TOCSY experiments confirmed its location at the C3 position. The conformation of the studied oligosaccharides was then inferred from the analysis of the vicinal coupling constants ($^3J_{HH}$) and NOE contacts. First, $^3J_{HH}$, containing information on ring puckering, was extracted from the 1D ^{1}H-NMR spectra. In both GlcNAc and GlcA rings, regardless of the sulfation pattern, the H1–H4 protons exhibited $^3J_{HH}$ values above 8.0 Hz, consistent with the *anti*-arrangement of vicinal protons and, therefore, with the predominance of the $^4C_1$ conformation. On the other hand, the values determined for $^3J_{H1H2}$ were in agreement with the α and β configurations of GlcNAc and GlcA rings, respectively (Fig. 2(ii)A).

The global conformations of the disaccharides **HDF-1** to **HDF-3** and **HDF-5** to **HDF-7** were investigated using NOESY experiments assisted by computational calculations.[12] The 2D NOESY spectrum obtained for **HDF-7** is shown in Fig. 2(ii)B, as an illustrative example, where key correlations defining the conformation of the disaccharide have been indicated (see Fig. 2(ii) B and C). The molecule displayed positive NOEs, in agreement with its small size and short rotational correlation time, as expected for a disaccharide. In addition, key intra-residue and inter-residue cross-peaks were identified, which allowed defining unequivocally the sugar conformation (Fig. 2(ii)B). Intra-residue NOE cross-peaks between H1–H3,

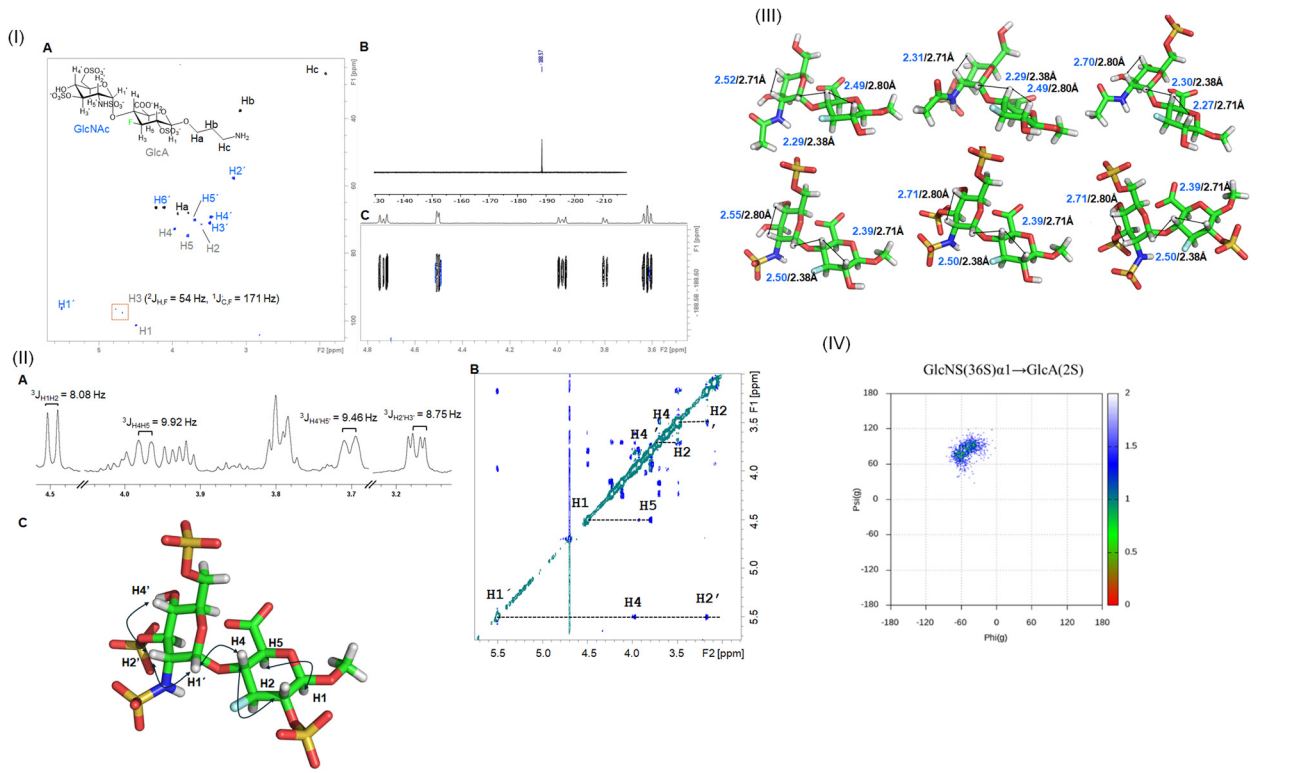

Fig. 2 Structural characterization of **HDF-7**: (i) NMR-based characterization of compound **HDF-7**. (A) ^{1}H–^{13}C-HSQC spectrum. ^{1}H-resonance assignment has been annotated: blue for GlcNAc, gray for GlcA, and black for the linker. (B) 1D ^{19}F-NMR spectrum of **HDF-7**. (C) 2D ^{19}F-relay-[H]H TOCSY spectrum; (ii) conformational analysis of compound **HDF-7**. (A) Expansion of the ^{1}H-NMR spectrum, showing the key ^{1}H resonances, where $^3J_{HH}$ values (Hz) have been indicated. (B) 2D NOESY spectra recorded for **HDF-7**. Relevant correlations are annotated. (C) Representative 3D model of **HDF-7**, generated using GLYCAM-Web tools and validated by NOE data; (iii) molecular models of fluorinated HS disaccharides. Key NOE-derived inter-proton distances (blue) are compared with theoretical values (black): (a) **HDF-1**, (b) **HDF-2,** (c) **HDF-3**, (d) **HDF-5**, (e) **HDF-6** and (f) **HDF-7**; (iv) docking and conformational analysis of the GlcNS(3S,6S)β1-4-GlcA(2S) disaccharide performed by MD simulations. Plots of ϕ/ψ values explored along the 100 ns MD trajectory are displayed. The points are colored as a function of the population density.

H1–H5 and H5–H3 proton pairs of GlcA were detected, indicative of the $^4C_1$ conformer. Although some overlapping occurs for GlcNAc protons signals, the NOE cross-peak for the H2–H4 proton pair was also observed, in agreement with the $^4C_1$ conformation. Fittingly, the inter-residue NOE contact between H1GlcNAc and H4GlcA was clearly detected, which is exclusive for the *exo-syn-*ϕ/*syn-*ψ conformation around the glycosidic linkage. Initial geometries for all compounds were built using the carbohydrate building module in the GLYCAM-Web portal. The disaccharide structures were then modified using the MAESTRO suite of programs to include a fluorine atom at position C3 and to display the corresponding sulfation pattern. Then, they were submitted to an energy minimization process with a low gradient convergence threshold (0.05) in 2500 steps, employing the AMBER force field.

Fittingly, the distances predicted from the molecular modelling approaches (in black) were in full agreement (Fig. 2(iii)) with those estimated experimentally by analysis of the NOEs (in blue), thus validating the modelling protocol. Tables with all experimental and theoretical inter-proton distances for disaccharides are included in the Materials and methods section. Collectively, the $^3J_{HH}$ values and NOE data are in agreement with the almost exclusive presence of a major conformer for all disaccharides, regardless of the sulfation pattern.

Overall, GlcNAc and GlcA residues behave as single $^4C_1$ chair conformation, and display the *exo-syn-*ϕ/*syn-*ψ conformation around the glycosidic linkage. Although no experimental data were recorded for the natural disaccharides (**HD1-14**), molecular dynamics (MD) simulations predicted a similar behavior to those observed for their fluorinated counterparts. In particular, 100 ns MD simulations for the GlcNS(3S,6S)β1-4-GlcA(2S) disaccharide (**HD-7** analog) predicted $^4C_1$ chairs for both pyranose rings and the *exo-syn-*ϕ/*syn-*ψ conformation as the major one around the glycosidic linkage (Fig. 2(iv)). Of note, although the conformation of **HDF-4** was not experimentally measured, it is anticipated to exhibit similar behaviour to the other analogues and is therefore not discussed in detail.

Next, to determine the effect of the fluorine substituent on protein binding to the HS disaccharidases, all the 7 HDFs (fluorinated) and 14 HDs (non-fluorinated HS disaccharides) were immobilised onto epoxy coated glycan microarray slides and binding patterns for 7 prominent human HS-binding growth factors and 9 chemokines were investigated as previously described:[10a–c] two fibroblast growth factors (**FGF1** and **FGF2**), two epidermal growth factors (**EGF** and **HB-EGF**), vascular endothelial growth factor (**VEGF**), amphiregulin and bone morphogenetic protein (**BMP2**). Each protein was tested at three different concentrations.

The resulting fluorescence intensities from the sub-arrays were normalised (expressed as a percentage of the maximum binding signal in each sub-array), averaged, and presented as a heatmap (Fig. 3a), as previously used to study carbohydrate–protein interactions.[11b,c,13] **EGF** showed minimal background fluorescence and was therefore excluded from analysis. The remaining six growth factors demonstrated binding preferences dependent on the sulfation pattern, fluorine substitution and the uronic acid composition of the HS disaccharides. Notably, **FGF1** exhibited unique and strong binding to the **HD-13** disaccharide ligand, but rather weak binding across other HS glycans, regardless of fluorination. This **FGF1** binding to **HD-13** is consistent with previously reported values.[14] In contrast, **FGF2** displayed a different binding pattern where it strongly bound both fluorinated and non-fluorinated disaccharides. It showed high binding preferences for non-fluorinated *N*-sulfated L-iduronic acid-based HS ligands—namely, **HD-13** and **HD-14** (ranking 82% and 85%, respectively), and some fluorinated mimetics exhibited similarly high binding preferences (**HDF-2**, **HDF-4** and **HDF-6**, ranging from 81 to 84%), while higher than their other non-fluorinated counterparts (**HD-6** and **HD-7**: ranking 77% and 70%, respectively). Likewise, **HDF-2**, which contains an *N*-acetyl domain, exhibited 84% ranking compared to 48% for its bioisosteric analogue **HD-2**. Furthermore, the increased degree of sulfation in fluorinated ligands led to enhanced binding: **HDF-4** bound at 81%, while *N*-sulfated analogues **HDF-6** and **HDF-7** showed binding of 84% and 72%, respectively. For $VEGF_{195}$, HB-EGF, amphiregulin, and BMP2, the fluorinated HS ligands (**HDF2–HDF7**) consistently exhibited stronger binding than their non-fluorinated equivalents (**HD2–HD7**). Nevertheless, among all disaccharides tested, highly sulfated L-iduronic acid-based **HD-13** and **HD-14** showed the strongest binding across most proteins, illustrating the preference of growth factors to L-iduronic acid over D-glucuronic acid, as previously suggested.[14,15] Collectively, these results prompted further investigation into the relationship between human FGF2 and fluorinated HS disaccharides, particularly in *N*-acetate domain D-glucuronic acid-based HS structures (**HDF-2** and **HDF-4**). To corroborate the binding specificity, we performed surface plasmon resonance (SPR) measurements between **FGF2** and **HDF-2**, **HDF-4**, and **HDF-6**, in comparison to **HD-14**. The SPR analysis demonstrated that all four disaccharides displayed similar affinities in the micromolar range (Fig. 3b and Table S7, ESI†), highlighting that the fluoro-HS mimetics, although not containing L-iduronic acid, can be used as higher affinity compounds. Although molecular modelling studies for the interaction between **FGF2** *vs.* **HDF-2** and **HDF-4** did not reveal further stabilizing contacts for the fluorinated analogues compared to the natural disaccharides, the incorporation of fluorine did not disrupt any long-lasting interaction (Fig. S1 and S2, ESI†). Notably, besides the hydrophobic contribution, non-bonding protein–fluorine interactions such as orthogonal CF–C═O(N) contacts, fluorine–nonpolar hydrogen contacts, and hydrogen bonds could be operative and potentially increased the binding affinity of the fluorinated mimetics. Finally, to further investigate the interaction between human **FGF2** and the fluorinated mimetics in biologically relevant context, cell proliferation and MAPK pathway activation assays were conducted with NIH-3T3 cells treated with human **FGF2** with and without exposure to the disaccharide mimetics. All four HS disaccharides (**HDF-2**, **HDF-4**, **HDF-6** and **HD-14**) displayed similar cell proliferation and MAPK activity, suggesting that the incorporation of a non-natural fluorine atom into

(a)

HD	Skeleton	Sulfation	Glycan Structure	FGF1	FGF2	VEGF	HB-EGF	Amphiregulin	BMP2
HDF-1	GlcNAc-GlcA	3F	GlcNAcα4GlcA(3F)βProNH2	0	10	0	7	14	2
HDF-2	GlcNAc-GlcA	6S−3F	GlcNAc(6S)α4GlcA(3F)βProNH2	1	84	53	72	60	83
HDF-3	GlcNAc-GlcA	3S−3F	GlcNAc(3S)α4GlcA(3F)βProNH2	0	74	45	48	59	73
HDF-4	GlcNAc-GlcA	6S,3S−2S,3F	GlcNAc(6S,3S)α4GlcA(2S,3F)βProNH2	20	81	65	70	54	63
HDF-5	GlcNS-GlcA	6S−3F	GlcNS(6S)α4GlcA(3F)βProNH2	5	76	66	68	43	66
HDF-6	GlcNS-GlcA	6S,3S−3F	GlcNS(6S,3S)α4GlcA(3F)βProNH2	23	84	60	64	40	64
HDF-7	GlcNS-Glc	6S,3S−2S,3F	GlcNS(6S,3S)α4GlcA(2S,3F)βProNH2	3	72	58	56	70	65
HD-1	GlcNAc-GlcA	None	GlcNAcα4GlcAβProNH2	0	2	0	4	4	2
HD-2	GlcNAc-GlcA	6S	GlcNAc(6S)α4GlcAβProNH2	0	48	26	47	30	32
HD-3	GlcNAc-GlcA	3S	GlcNAc(3S)α4GlcAβProNH2	0	35	23	20	35	21
HD-4	GlcNS-GlcA	6S	GlcNS(6S)α4GlcAβProNH2	2	70	48	61	60	55
HD-5	GlcNS-GlcA	3S	GlcNS(3S)α4GlcAβProNH2	7	79	59	70	49	61
HD-6	GlcNS-GlcA	6S,3S	GlcNS(6S,3S)α4GlcAβProNH2	13	77	57	54	61	54
HD-7	GlcNS-GlcA	6S,3S−2S	GlcNS(6S,3S)α4GlcA(2S)βProNH2	19	70	53	47	51	48
HD-8	GlcNAc-IdoA	None	GlcNAcα4IdoAαProNH2	0	24	20	7	34	19
HD-9	GlcNAc-IdoA	6S	GlcNAc(6S)α4IdoAαProNH2	0	41	35	31	35	26
HD-10	GlcNAc-IdoA	3S	GlcNAc(3S)α4IdoAαProNH2	0	41	28	26	29	32
HD-11	GlcNS-IdoA	6S	GlcNS(6S)α4IdoAαProNH2	1	70	35	56	46	58
HD-12	GlcNS-IdoA	3S	GlcNS(3S)α4IdoAαProNH2	1	61	30	30	59	46
HD-13	GlcNS-IdoA	6S−2S	GlcNS(6S)α4IdoA(2S)αProNH2	90	82	90	91	73	71
HD-14	GlcNS-IdoA	6S,3S−2S	GlcNS(6S,3S)α4IdoA(2S)αProNH2	30	85	87	66	65	83
Heparin	N/A	Complex	Heparin	48	34	22	5	19	13

Rank (%): 100, 75, 50, 25, 0

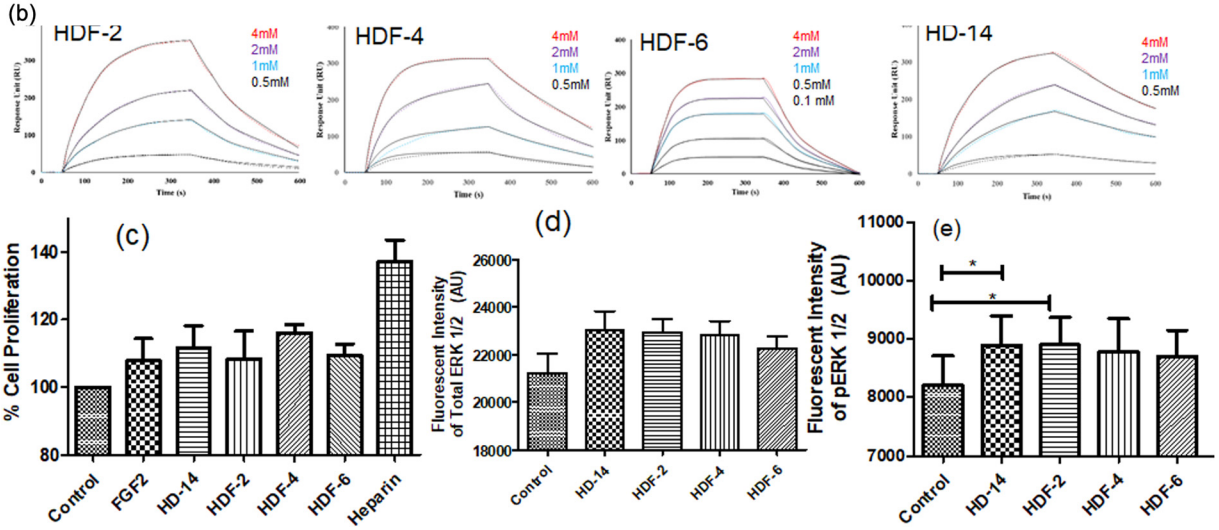

Fig. 3 Growth factors binding to **HD** and **HDF** mimetics: (a) HS disaccharide mimetics glycan microarray analysis of human FGF1, FGF2, $VEGF_{195}$, HB-EGF, amphiregulin and BMP2. All proteins were tested at three concentrations (10, 3.3, and 1.6 ng μl^{-1}), each per sub-array. Binding was tested with biotinylated secondary antibodies and then detected with Cy3-streptavidin. Relative fluorescence units (RFU) were ranked according to the highest signal in each sub-array, and then ranks of all examined concentrations was averaged and plotted as a heatmap (red, highest rank; white, 50th percentile; and blue, lowest rank). (b) Human FGF2 SPR binding analysis with **HDF-2**, **HDF-4**, **HDF-6** and **HD-14**. FGF2 concentrations ranged from 0.1 to 4 mM, and a global fit according to a 1 : 1 binding model was applied (black curves); the dissociation constant (K_D) for **HDF-2** is 72 ± 0.63 μM; the dissociation constant for **HDF-4** is 71 ± 0.61; the dissociation constant for **HDF-6** is 89 ± 0.36 and the dissociation constant for **HD-14** is 64 ± 0.12; (c) NIH-3T3 WST cell proliferation assay. Cells were seeded on a HS disaccharide coated 96-well plate and treated with FGF2 (10 ng ml^{-1}). Control wells (without disaccharide or FGF2) were used as baseline for proliferation (set as 100%) and then quantified after 48 h. Statistics (mean ± SD) was performed in triplicate. (d) MAPK pathway activation assay. NIH-3T3 cells were seeded on a HS disaccharide coated 96-well plate (along with wells with no disaccharides as control), and treated with FGF2 (50 ng ml^{-1}) or PBS for control, and total ERK1/2 and pERK1/2 were quantified by respective fluorescently labeled antibodies. All statistical analyses were performed using GraphPad Prism 5. Significant differences between control and HS mimetics are indicated with asterisk (*$p < 0.05$), and data are expressed as mean ± SD ($n = 4$), using one-way ANOVA.

N-acetylated HS mimetics did not interfere with the biological activity of the cells (Fig. 3c–e).

Next, nine human chemokines were examined by the glycan HS mimetics microarray (Fig. 4): three homeostatic chemokines (**CCL28**, **CXCL12**, and **CCL21**) and six inflammatory chemokines [**CXCL13**, **CXCL10** (IP-10), **CCL2** (MCP-1), **CCL7** (MCP-3), **CCL13** (MCP-4), and **CCL5** (RANTES)]. Glycan microarray analysis showed that overall, all chemokines, but **CXCL13**, bound well to the fluorinated mimetics. Human **CCL13** showed the widest recognition profile, with high binding to all fluorinated and sulfated HS mimetics and top binding to highly sulfated L-iduronic acid containing HS mimetics (**HD-13** and **HD-14**). Similarly, all the other inflammatory chemokines (**CXCL10**, **CCL7**, **CCL2**, and **CCL5**) showed the highest binding to **HD-13** and **HD-14** and also recognized the 6-*O*-sulfated fluorinated mimetics (**HDF-2** to **HDF-7**) well, slightly better

HD	Skeleton	Sulfation	Glycan Structure	CCL13	CXCL10	CCL7	CCL2	CXCL12	CCL5	CCL28	CCL21	CXCL13
HDF-1	GlcNAc-GlcA	3F	GlcNAcα4GlcA(3F)βProNH2	12	4	0	0	2	1	2	0	0
HDF-2	GlcNAc-GlcA	6S−3F	GlcNAc(6S)α4GlcA(3F)βProNH2	72	75	66	51	61	35	41	76	5
HDF-3	GlcNAc-GlcA	3S−3F	GlcNAc(3S)α4GlcA(3F)βProNH2	72	34	32	37	50	34	19	34	5
HDF-4	GlcNAc-GlcA	6S,3S−2S,3F	GlcNAc(6S,3S)α4GlcA(2S,3F)βProNH2	74	81	69	77	67	55	43	34	48
HDF-5	GlcNS-GlcA	6S−3F	GlcNS(6S)α4GlcA(3F)βProNH2	66	61	61	61	47	47	34	34	11
HDF-6	GlcNS-GlcA	6S,3S−3F	GlcNS(6S,3S)α4GlcA(3F)βProNH2	62	45	40	69	65	61	25	28	30
HDF-7	GlcNS-Glc	6S,3S−2S,3F	GlcNS(6S,3S)α4GlcA(2S,3F)βProNH2	71	68	52	62	52	37	33	53	11
HD-1	GlcNAc-GlcA	None	GlcNAcα4GlcAβProNH2	1	2	0	0	1	0	0	0	3
HD-2	GlcNAc-GlcA	6S	GlcNAc(6S)α4GlcAβProNH2	50	47	37	16	51	22	20	62	6
HD-3	GlcNAc-GlcA	3S	GlcNAc(3S)α4GlcAβProNH2	45	39	31	21	43	29	16	54	1
HD-4	GlcNS-GlcA	6S	GlcNS(6S)α4GlcAβProNH2	56	60	49	45	54	36	30	51	7
HD-5	GlcNS-GlcA	3S	GlcNS(3S)α4GlcAβProNH2	65	52	43	46	54	47	19	51	9
HD-6	GlcNS-GlcA	6S,3S	GlcNS(6S,3S)α4GlcAβProNH2	65	62	62	59	56	54	41	38	17
HD-7	GlcNS-GlcA	6S,3S−2S	GlcNS(6S,3S)α4GlcA(2S)βProNH2	69	54	56	60	53	61	35	31	28
HD-8	GlcNAc-IdoA	None	GlcNAcα4IdoAαProNH2	27	27	14	10	19	13	27	10	3
HD-9	GlcNAc-IdoA	6S	GlcNAc(6S)α4IdoAαProNH2	45	31	30	11	46	19	10	39	3
HD-10	GlcNAc-IdoA	3S	GlcNAc(3S)α4IdoAαProNH2	48	62	46	19	46	16	29	39	4
HD-11	GlcNS-IdoA	6S	GlcNS(6S)α4IdoAαProNH2	54	46	50	19	58	39	17	55	3
HD-12	GlcNS-IdoA	3S	GlcNS(3S)α4IdoAαProNH2	42	49	37	16	47	34	8	40	4
HD-13	GlcNS-IdoA	6S−2S	GlcNS(6S)α4IdoA(2S)αProNH2	91	56	75	74	84	65	64	43	95
HD-14	GlcNS-IdoA	6S,3S−2S	GlcNS(6S,3S)α4IdoA(2S)αProNH2	80	88	77	77	69	60	56	39	51
Heparin	N/A	Complex	Heparin	27	59	72	32	29	65	15	66	65

Rank (%): 100, 75, 50, 25, 0

Fig. 4 Chemokines binding to **HD** and **HDF** mimetics: (a) HS disaccharide mimetics microarray analysis of human CCL13, CXCL10, CCL7, CCL2, CXCL12, CCL5, CCL28, CCL21, and CXCL13. All proteins were tested at three concentrations (10, 3.3 and 1.6 ng μl^{-1}) each per sub-array. Binding was tested with biotinylated secondary antibodies and then detected with Cy3-streptavidin. Relative fluorescence units (RFU) were ranked according to the highest signal in each sub-array, and then ranks of all of the examined concentrations were averaged and plotted as a heatmap (red, highest rank; white, 50th percentile; blue, lowest rank).

than the non-fluorinated disaccharides (**HD-2** to **HD-7**). Each of the hemostatic chemokines showed different binding patterns. Human **CCL28** preferred **HD13** and **HD-14** with only lower ranked binding to the 6-*O*-sulfated fluorinated mimetics **HFD-2** and **HFD-4** and to the non-fluorinated glycan **HD-6**. Interestingly, human **CCL21** top ranked glycan was **HFD-2**, whereas **CXCL13** preferred **HD-13** with lower preference to **HD-14** and **HFD-4**. Further research is needed to determine whether these preferences can be exploited to design HS mimetics for glycotherapy.

Conclusions

We herein reported a divergent strategy to synthesize a first generation of fluorinated HS disaccharide ligands having both *N*-acetate and *N*-sulfated glucosamine moieties. ^{19}F-NMR studies have shown that the chemical shifts are sensitive to the sulfation pattern. Highly sulfated ligands showed upward shifts compared to low or non-sulfated HS ligands. Conformation plasticity analysis of fluorinated HS showed that all compounds keep the canonical $^{4}C_{1}$-glucuronic acid conformation. Finally, a systematic glycan microarray and SPR analysis showed that fluorine edition to HS mimetics significantly modulates the binding preferences compared with the low-sulfated HS ligands to growth factors and chemokines. Molecular modelling studies of the interaction between FGF2 and HDF analogs suggest that the newly synthesized molecules bind to the protein with a binding mode similar to the natural disaccharides. These results suggest that fluorinated heparan sulfate (HS) ligands may exhibit distinct and modular binding interactions with growth factors and chemokines compared to their native counterparts. While the current study provides important initial insights, the use of higher oligosaccharides may offer a more comprehensive understanding of these interactions. Ongoing work in our laboratory is focused on extending this approach to higher-order HS structures.

Author contributions

R. K., J. J. B. and V. P. K. planned the project, analysed data, and wrote manuscript with some assistance from other co-authors. V. M., R. R., S. A., S. M., and A. C. synthesized, purified, and characterized the HS ligands and performed all assays. P. G. and A. G. performed conformation studies. S. L. B.-A. performed HS-protein binding assay on microarrays and critically reviewed the manuscript.

Conflicts of interest

The authors declare no conflict of interest.

Data availability

The data supporting this article have been included as part of the ESI.†

Acknowledgements

Financial support from the IISER, Pune (to S. A.), DBT (grant nos. BT/PR21934/NNT/28/1242/2017, STARS/APR2019/CS/426/FS, and SERB/F/9228/2019-2020) and DST WOS-A grant (CS-72-2019) (to R. K. and P. R. B. respectively), and the Israel Science Foundation—Israel Precision Medicine Program (ISF-IPMP no. 3042/22) and the European Research Council Consolidator Grant ERC-2020-COG-101003021 (to V. P.-K.) is gratefully acknowledged. A. G. and J. J. B. are thankful to Agencia Estatal de Investigación of Spain for grants PID2023-150779OA-I00 (A. G.), PDI2021-1237810B-C21

(J. J. B.), and the Severo Ochoa Center of Excellence Accreditation CEX2021-001136-S, funded through the grant MCIN/AEI/10.13039/501100011033. This work is dedicated to the memory of Prof. Robert J. Linhardt for his outstanding contributions to heparan sulfate glycobiology.

References

1 (*a*) D. Xu and J. D. Esko, *Annu. Rev. Biochem.*, 2014, **83**, 129–157; (*b*) I. Vlodavsky, M. Gross-Cohen, M. Weissmann, N. Ilan and R. D. Sanderson, *Trends Biochem. Sci.*, 2018, **43**, 18–31; (*c*) I. Capila and R. J. Linhardt, *Angew. Chem., Int. Ed.*, 2002, **41**, 390–412.

2 (*a*) J. M. Whitelock and R. V. Iozzo, *Chem. Rev.*, 2005, **105**, 2745–2764; (*b*) U. Lindahl, J. Couchman, K. Kimmata and J. D. Esko, *Essentials of Glycobiology*, ed.A. Varki, R. D. Cummings, J. D. Esko, P. Stanley, G. W. Hart, M. Aebi, A. G. Darvill, T. Kinoshita, N. H. Packer, J. H. Prestegsard, R. L. Schnaarand, P. H. Seeberger, Cold spring Harbor Laboratory press, 3rd edn, 2017.

3 (*a*) K. Sakamoto, T. Ozaki, Y.-C. Ko, C.-F. Tsai, Y. Gong, M. Morozumi, Y. Ishikawa, K. Uchimura, S. Nadanaka and H. Kitagawa, *Nat. Chem. Biol.*, 2019, **15**, 699–709; (*b*) M. C. Meneghetti, A. J. Hughes, T. R. Rudd, H. B. Nader, A. K. Powell, E. A. Yates and M. A. Lima, *J. R. Soc. Interface.*, 2015, **12**, 20150589; (*c*) J. R. Bishop, M. Schuksz and J. D. Esko, *Nature*, 2007, **446**, 1030–1037; (*d*) M. M. L. Zulueta, C.-L. Chyan and S.-C. Hung, *Curr. Opin. Struct. Biol.*, 2018, **50**, 126–133; (*e*) P. Wang, F. L. Cascio, J. Gao, R. Kayed and X. Huang, *Chem. Commun.*, 2018, **54**, 10120–10123; (*f*) M. M. L. Zulueta, S.-Y. Lin, Y.-T. Lin, C.-J. Huang, C.-C. Wang, C.-C. Ku, Z. Shi, C.-L. Chyan, D. Irene and L.-H. Lim, *J. Am. Chem. Soc.*, 2012, **134**, 8988–8995; (*g*) Z. Wang, P.-H. Hsieh, Y. Xu, D. Thieker, E. J. E. Chai, S. Xie, B. Cooley, R. J. Woods, L. Chi and J. Liu, *J. Am. Chem. Soc.*, 2017, **139**, 5249–5256; (*h*) A. Pozzi, P. D. Yurchenco and R. V. Iozzo, *Matrix. Biol.*, 2017, **57–58**, 1–11; (*i*) A. Mantovani, R. Bonecchi and M. Locati, *Nat. Rev. Immunol.*, 2006, **6**, 907–918; (*j*) C. R. Mackay, *Nat. Immunol.*, 2001, **2**, 95–101; (*k*) R. J. Nibbs and G. J. Graham, *Nat. Rev. Immunol.*, 2013, **13**, 815–829.

4 (*a*) F. L. Kearns, D. R. Sandoval, L. Casalino, T. M. Clausen, M. A. Rosenfeld, C. B. Spliid, R. E. Amaro and J. D. Esko, *Curr. Opin. Struct. Biol.*, 2022, **76**, 102439; (*b*) M. Chhabra, G. D. Doherty, N. W. See, N. S. Ghandi and V. Ferro, *Chem. Rec.*, 2021, **21**, 3087–3101; (*c*) P. Chopra, T. Yadavalli, F. Palmieri, S. A. K. Jongkees, L. Unione, D. Shukla and G. J. Boons, *Angew. Chem., Int. Ed.*, 2023, **62**, e202309838.

5 (*a*) S. Ramadan, M. Mayieka, N. L. B. Pohl, J. Liu, L. C. Hsieh-wilson and X. Huang, *Curr. Opion. Chem. Biol.*, 2024, **80**, 102455; (*b*) N. J. Pawar, L. Wang, T. Higo, C. Bhattacharya, P. K. Kancharla, F. Zhang, K. Baryal, C. X. Huo, J. Liu, R. J. Linhardt, X. Huang and L. C. Hsieh-Wilson, *Angew. Chem., Int. Ed.*, 2019, **58**, 18577–18583; (*c*) L. Wang, A. W. Sorum, B. S. Huang, M. K. Kern, G. Su, N. Pawar, X. Huang, J. Liu, N. L. B. Pohl and L. C. Hsieh-Wilson, *Nat. Chem.*, 2023, **15**, 1108–1117.

6 (*a*) B. E. Thacker, E. Seamen, R. Lawrence, M. W. Parker, Y. Xu, J. Liu, C. W. V. Kooi and J. D. Esko, *ACS Chem. Bio.*, 2016, **11**, 971–980; (*b*) H. Ham, Y. Xu, C. A. Haller, E. Dai, E. STancanelli, J. Liu and E. L. Chaikof, *J. Med. Chem.*, 2023, **66**, 2194–2203; (*c*) C. D. O'Donnell, M. Kovacs, J. Akhtar, T. Valyi-Nagy and D. Shukla, *Virology*, 2010, **397**, 389–398.

7 (*a*) S. E. Stringer and J. T. Gallagher, *J. Biol. Chem.*, 1997, **272**, 20508–20514; (*b*) D. Spillmann, D. Witt and U. Lindahl, *J. Biol. Chem.*, 1998, **273**, 15487–15493; (*c*) G. C. Jayson, S. U. Hansen, G. J. Miller, C. L. Cole, G. Rushton, E. Avizienyte and J. M. Gardiner, *Chem. Commun.*, 2015, **51**, 13846–13849; (*d*) G. J. Sheng, Y. I. Oh, S.-K. Chang and L. C. Hsieh-Wilson, *J. Am. Chem. Soc.*, 2013, **135**, 10898–10901; (*e*) J. L. de Paz, E. A. Moseman, C. Noti, L. Polito, U. H. von Andrian and P. H. Seeberger, *ACS Chem. Biol.*, 2007, **2**, 735–744; (*f*) L. Liu, P. Chopra, X. Li, K. M. Bouwman, S. M. Tompkins, M. A. Wolfert, R. P. de Vries and G. J. Boons, *ACS Cent. Sci.*, 2021, **7**, 1009–1018.

8 (*a*) F. Demeter, T. Demeter, Z. Bereczky, K. E. Kövér, M. Herczeg and A. Borbás, *Sci. Rep.*, 2018, **8**, 13736; (*b*) M. Herczeg, F. Demeter, E. Lisztes, M. Racskó, B. I. Tóth, I. Timári, Z. Bereczky, K. E. Kövér and A. Borbás, *J. Org. Chem.*, 2022, **87**, 15830–15836; (*c*) S. K. Das, J. M. Mallet, J. Esnault, P. A. Driguez, P. Duchaussoy, P. Sizun, J. P. Herault, J. Herbert, M. Petitou and P. Sinaÿ, *Chem. – Eur. J.*, 2001, **7**, 4821–4834.

9 (*a*) S. J. Richards, T. Keenan, J. B. Vendeville, D. E. Wheatley, H. Chidwick, D. Budhadev, C. E. Council, C. S. Webster, H. Ledru, A. N. Baker, M. Walker, M. C. Galan, B. Linclau, M. A. Fascione and M. I. Gibson, *Chem. Sci.*, 2021, **12**, 905; (*b*) R. Hevey, *Chem. – Eur. J.*, 2021, **27**, 2240–2253; (*c*) B. Linclau, A. Ardá, N. C. Reichardt, M. Sollogoub, L. Unione, S. P. Vincent and J. J. Barbero, *Chem. Soc. Rev.*, 2020, **49**, 3863; (*d*) K. Huonnic and B. Linclau, *Chem. Rev.*, 2022, **122**, 15503–15602; (*e*) K. Hollingsworth, A. D. Maio, S. J. Richards, J. B. Vendeville, D. E. Wheatley, C. E. Council, T. Keenan, H. Ledru, H. Chidwick, K. Huang, F. Parmeggiani, A. Marchesi, W. Chai, R. McBerney, T. P. Kaminski, M. R. Balmforth, A. Tamasanu, J. D. Finnigan, C. Young, S. L. Warriner, M. E. Webb, M. A. Fascione, S. Flitsch, M. C. Galan, T. Ferizi, M. I. Gibson, Y. Liu, W. B. Turnbull and B. Linclau, *Nat. Commun.*, 2024, **15**, 7925; (*f*) V. Denavit, D. Lainé, C. Bouzriba, E. Shanina, E. Gillon, S. Fortin, C. Rademacher, A. Imberty and D. Giguére, *Chem. Eur. J.*, 2019, **25**, 4478–4490; (*g*) G. Fittolani, E. Shanina, M. Guberman, P. H. Seeberger, C. Rademacher and M. Delbianco, *Angew. Chem., Int. Ed.*, 2021, **60**, 13302–13309; (*h*) J. P. Snyder, N. S. Chadrakumar, H. Sato and D. C. Lankin, *J. Am. Chem. Soc.*, 2000, **122**, 544–545.

10 (*a*) R. F. Flavell, C. Trillet, M. K. Regan, T. Ganguly, J. E. Blecha, J. Kurhanewicz, H. F. VanBrocklin, K. R. Keshari, C. J. Chang, M. J. Evans and D. M. Wilson, *Bioconj. Chem.*, 2016, **27**, 170–178; (*b*) M. Kalita, J. Villanueva-Meyer, Y. Ohkawa, C. Kalyanaraman, K. Chen, E. Mohamed,

M. F. L. Parker, M. P. Jacobson, J. J. Phillips, M. J. Evans and D. M. Wilson, *Mol. Pharm.*, 2021, **18**, 451–460; (*c*) K. Siebold, E. chikunova, N. Lorz, C. Jordan, A. D. Gossert and R. Gilmour, *Angew. Chem., Int. Ed.*, 2025, **64**, e20243782; (*d*) E. Campbell, C. Jordan and R. Gilmour, *Chem. Soc. Rev.*, 2023, **52**, 3599–3626; (*e*) C. S. Teschers and R. Gilmour, *Angew. Chem., Int. Ed.*, 2023, **62**, e202213304; (*f*) T. Hayashi, G. Kehr, K. Bergander and R. Gilmour, *Angew. Chem., Int. Ed.*, 2019, **58**, 3814–3818; (*g*) A. R. Hewson, H. O. Lloyd-laney, T. Keenan, S. J. Richards, M. I. Gibson, B. Linclau, N. Signoret, M. A. FAscione and A. Parkin, *Chem. Sci.*, 2024, **15**, 16086–16095.

11 (*a*) P. Jain, D. Shanthamurthy, P. M. Chaudhary and R. Kikkeri, *Chem. Sci.*, 2021, **12**, 4021–4027; (*b*) P. Jain, C. D. Shanthamurthy, S. L. Ben-Arye, R. J. Woods, R. Kikkeri and V. Palder-Karavani, *Chem. Sci.*, 2021, **12**, 3674–3681; (*c*) P. Jain, C. D. Shanthamurthy, S. L. Ben-Arye, S. Yehuda, S. S. Nandikol, H. V. Thulasiram, V. Padler-Karavani and R. Kikkeri, *Chem. Commun.*, 2021, **57**, 3516–3519; (*d*) S. Anand, P. R. Bhoge, R. Raigwali, S. V. Saladi and R. Kikkeri, *Chem. Sci.*, 2024, **15**, 19962–19969.

12 J. Angulo, A. Ardá, S. Bertuzzi, A. Canales, J. Ereño-Orbea, A. Gimeno, M. Gomez-Redondo, J. C. Muñoz-García, P. Oquist, S. Monaco, A. Poveda, L. Unione and J. Jiménez-Barbero, *Prog. Nucl. Magn. Reson. Spectrosc.*, 2024, **144–145**, 97–152.

13 (*a*) C. D. Shanthamurthy, A. Gimeno, S. Leviatan Ben-Arye, N. V. Kumar, P. Jain, V. Padler-karavan, J. Jiménez-Barbero and R. Kikkeri, *ACS Chem. Biol.*, 2021, **16**, 2481–2489; (*b*) C. D. Shanthamurthy, S. Leviatan Ben-Arye, N. V. Kumar, S. Yehuda, R. Amon, R. J. Woods, V. Padler-Karavani and R. Kikkeri, *J. Med. Chem.*, 2021, **64**, 3367–3380.

14 (*a*) Y. C. Li, I. H. Ho, C. C. Ku, Y. Z. Zhong, Y. P. Hu, Z. G. Chen, C. Y. Chen, W. C. Lin, M. M. Zulueta, S. C. Hung, M. G. Lin, C. C. Wang and C. D. Hsiao, *ACS Chem. Biol.*, 2014, **9**, 1712–1717; (*b*) J. P. Shaw, Z. Johnson, F. Borlat, C. Zwahlen, A. Kungl, K. Roulin, A. Harrenga, T. N. C. Wells and A. E. I. Proudfoot, *Structure*, 2004, **12**, 2081–2093.

15 (*a*) Y. P. Hu, Y. Q. Zhong, Z. G. Chen, C. Y. Chen, Z. Shi, M. M. Zulueta, C. C. Ku, P. Y. Lee, C. C. Wang and S. C. Hung, *J. Am. Chem. Soc.*, 2012, **134**, 20722–20727; (*b*) C. C. Melo-Filho, G. Su, K. Liu, E. N. Muratov, A. Tropsha and J. Liu, *Glycobiology*, 2024, **34**, cwae039; (*c*) S. Gulieri, M. Hricovíni, R. Raman, L. Polito, G. Torri, B. Casu, R. Sasisekharan and M. Guerrini, *Biochemistry*, 2008, **47**(52), 13862–13869.